

# $\Phi^4$ theory on the lattice

Max Jansen, Kilian Nickel

March 2011



# Contents

<b>1</b>	<b>Motivation</b>	<b>1</b>
<b>2</b>	<b>Theory</b>	<b>1</b>
2.1	Path integral . . . . .	1
2.2	Renormalization . . . . .	1
2.3	Spontaneous symmetry breaking (SSB) . . . . .	3
2.4	Effective Potential . . . . .	3
<b>3</b>	<b>Algorithm</b>	<b>5</b>
<b>4</b>	<b>Data analysis</b>	<b>6</b>
4.1	Mass calculation . . . . .	6
4.2	Effective potential . . . . .	9
4.2.1	Errors of numerically calculated $V_{\text{eff}}$ . . . . .	11
4.3	Renormalized coupling constant . . . . .	12
4.4	Finite size effects . . . . .	14
<b>5</b>	<b>Error analysis</b>	<b>14</b>
5.1	Standard deviation . . . . .	14
5.2	Autocorrelation . . . . .	15
<b>6</b>	<b>Summary</b>	<b>15</b>

# 1 Motivation

The theory described by the Lagrangian

$$\mathcal{L} = \frac{1}{2}(\partial\phi)^2 - \frac{1}{2}\mu^2\phi^2 - \frac{\lambda}{4!}\phi^4 \quad (1.1)$$

is the simplest case of an interacting quantum field theory with a real field  $\phi$ . It serves as a toy model to study the principles of quantum field theory, especially renormalization. Its physical importance lies in its application in the Standard Model, where the Higgs field is described by (1.1), only with the difference that the Higgs field is a complex doublet.

## 2 Theory

### 2.1 Path integral

The path integral formulation of  $\phi^4$  theory is the foundation of our algorithm. The main quantity is the vacuum-to-vacuum transition amplitude  $Z[J]$  with an additional source  $J(x)$  coupled to the field  $\phi(x)$ . This source is a tool to extract theoretically useful quantities out of the functional  $Z[J]$ .

$$Z[J] = \langle 0 | e^{-iHT} | 0 \rangle = \int \mathcal{D}\phi e^{i \int d^4x (\mathcal{L} + J\phi)} \quad (2.1)$$

The time  $T$  is understood to go to  $\infty$ . The functional integral runs over all possible functions  $\phi(x)$  and is in general not solvable. This is why theorists are forced to do perturbation theory by expanding the exponential. By going to a field on a lattice, we can generate some field configuration and evaluate the integrand numerically. Since complex numbers should not appear in our calculation, we introduce imaginary time  $t = -i\tau$ . This gives the substitutions  $\partial_t = i\partial_\tau$  and  $dt = -id\tau$ . Also the time integration range rotates into the imaginary axis. If the integrand is holomorphic, the time range can be shifted back to the real axis again, so that the integration still runs over the whole real spacetime. This procedure is called Wick rotation. The derivatives now read

$$(\partial\phi)^2 = -((\partial_\tau\phi)^2 + (\nabla\phi)^2) \quad (2.2)$$

like an Euclidean metric. We can now write down the vacuum amplitude

$$Z[J] = \int \mathcal{D}\phi e^{-S_E(J)} \quad (2.3)$$

in terms of the Euclidean action  $S_E$

$$S_E = \int d^4x \left( \frac{1}{2} ((\partial_t\phi)^2 + (\nabla\phi)^2) + \frac{\mu^2}{2}\phi^2 + \frac{\lambda}{4!}\phi^4 - J\phi \right). \quad (2.4)$$

Most of the field configurations have very high actions and don't contribute to the integral because  $e^{-S_E}$  is very small. We do importance sampling using a Metropolis algorithm, where the field is sampled according to the distribution  $e^{-S_E}$ .

### 2.2 Renormalization

The propagator associated with an internal line in a Feynman diagram is  $D(p) = i/(p^2 - m^2 + i\epsilon)$  at lowest order. When evaluating  $n$ -point correlation functions by differentiating the amplitude  $Z[J]$  (c.f. Ryder[R]), e.g. the 2-point function, one obtains a series of loop diagrams shown in fig. 1 (these are only composed of 1-particle-irreducible diagrams of first order).

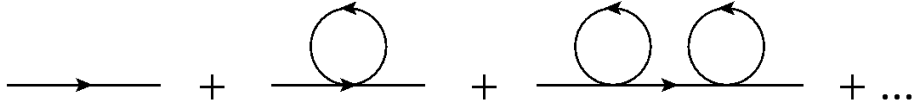


Fig. 1: Loop diagrams of the 2-pt. function

If the second diagram of this series gives a correction  $-i\Sigma$  to the propagator  $D(p)$ , then the sum is

$$D(p) + D(p)(-i\Sigma)D(p) + D(p)(-i\Sigma)D(p)(-i\Sigma)D(p) + \dots = \frac{i}{p^2 - (m^2 + \Sigma) + i\epsilon} \quad (2.5)$$

by virtue of the geometric series. This leads to a redefinition of the mass, known as mass shift  $m_r^2 = m^2 + \Sigma$ . In our case,  $\mu^2$  is  $m^2$ , but  $m$  is the letter used throughout in literature. The quadratic mass shift explains, why symmetry breaking is observed for negative  $\mu^2 < \mu_0^2$  with  $\mu_0^2 < 0$  instead of  $\mu_0^2 = 0$ . We will focus on this fact in the following sections.

Similarly, when the 4-point corrections are calculated from second order diagrams like those in fig. 2 for the  $s$ ,  $t$  and  $u$  channel, the coupling constant receives a shift. The resulting renormalized coupling  $\lambda_r$  is the physical one.

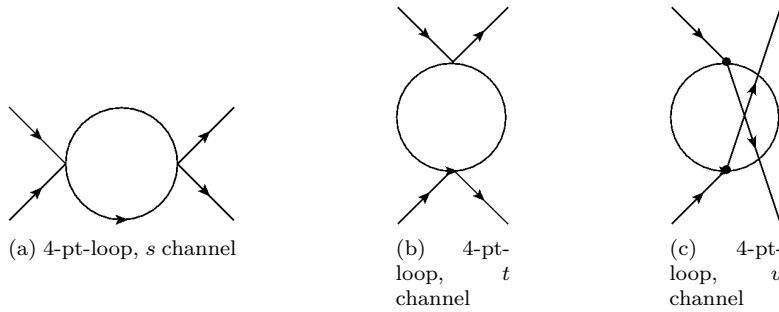


Fig. 2: 4-point corrections, one loop

In the cutoff renormalization scheme a cutoff momentum  $\Lambda$  is introduced to display infinite integrals. It is interpreted as a scale up to which the theory is valid. It is, however, not a physical quantity and all physical quantities should not depend on it. On a lattice, such a cutoff is naturally defined by the finite lattice spacing  $a$ . This is explained in figure 3: The field  $\phi$  is equivalent to a collection of anharmonic springs in spacetime, represented by the dots. The red wave can be resolved, but the blue wave with a higher frequency would look the same. The red wave defines a momentum cutoff which is proportional to  $1/a$ .

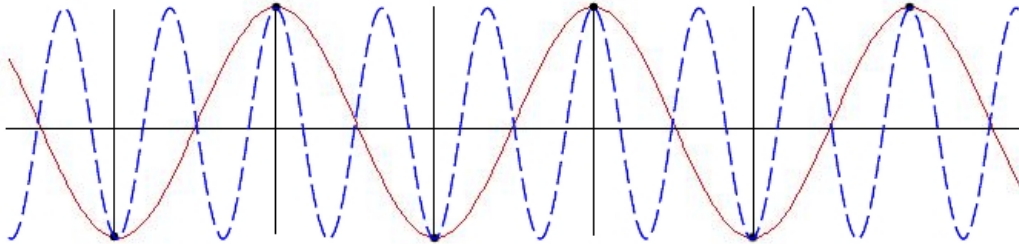


Fig. 3: Finite lattice spacing

## 2.3 Spontaneous symmetry breaking (SSB)

The Lagrangian of the  $\phi^4$  theory is

$$\mathcal{L} = \frac{1}{2} (\partial\phi)^2 - \frac{\mu^2}{2} \phi^2 - \frac{\lambda}{24} \phi^4, \quad (2.6)$$

where  $\lambda$  and  $\mu$  are arbitrary, unrenormalized parameters of the theory with no physical meaning.

For  $\lambda < 0$ , the potential would not be bound from below and the ground state indefinite. Thus the case  $\lambda < 0$  will not be considered in the following discussion.

For  $\mu^2, \lambda > 0$ , the potential is of the form shown in figure 4. The ground state is at  $\phi = 0$ , thus has a  $\mathbb{Z}_2$ -symmetry and the vacuum expectation value (vev) of the field is zero, although there may be quantum fluctuations.

Now let  $\mu^2 < 0, \lambda > 0$ . The unrenormalized potential is exemplarily shown in figure 5. The state at  $\phi = 0$  is unstable and there are two ground states with a vev  $\langle\phi\rangle \neq 0$ .

Replacing the scalar field  $\phi$  by a complex  $\mathbb{C}^2$  field  $\Phi$  and introducing a Yukawa interaction term  $\mathcal{L}_{\text{Yuk,int}} = g\bar{\psi}\Phi\psi$ , with fermion fields  $\psi$ , the fermion and W,Z boson masses in the Standard Model can be explained.

Back to scalar field theory. Even though the unrenormalized potential may have a minimum at  $\phi \neq 0$ , the mass shift can be large enough, such that the renormalized potential has one minimum at  $\phi = 0$ . In this case, no spontaneous symmetry breaking will occur.

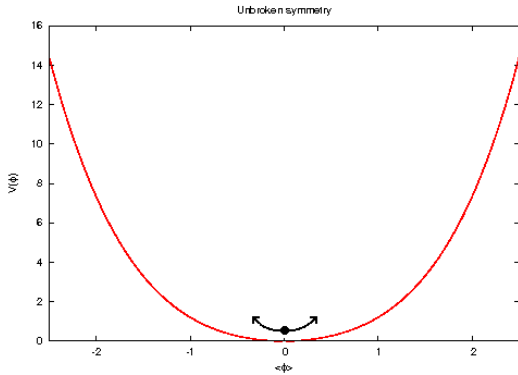


Fig. 4: Unbroken symmetry

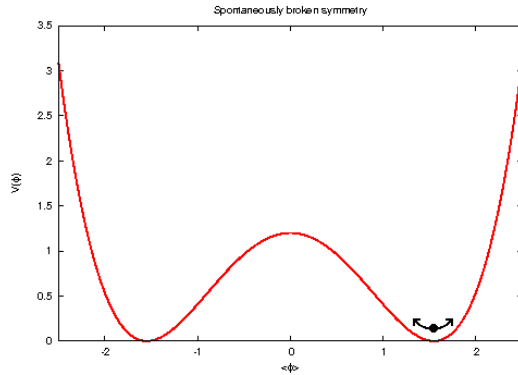


Fig. 5: Spontaneously broken symmetry

For further discussion c.f Peskin/Schroeder (1995).[PS]

## 2.4 Effective Potential

The effective potential is introduced to describe theories with spontaneously broken symmetries in the same manner as those without symmetry breaking. With knowledge of the effective potential one can determine the renormalized mass and coupling constant as well as the field strength renormalization constant.

To calculate the effective potential, bring in the external source  $J$ . Define  $U(\phi)$  to be:

$$U(\phi) = V(\phi) - J\phi \quad (2.7)$$

where  $J$  does not depend on  $\phi$ . Now let  $\langle\phi\rangle \equiv \langle\phi\rangle(J)$  be the expectation value in presence of the external source, hence, by inverting,  $J \equiv J(\langle\phi\rangle)$ .  $U(\phi)$  has a minimum at  $\langle\phi\rangle$  and therefore

$$\frac{\partial U}{\partial\phi}(\langle\phi\rangle) = 0 = \frac{\partial V}{\partial\phi}(\langle\phi\rangle) - J(\langle\phi\rangle) \quad (2.8)$$

Since we are on the lattice, we measure only renormalized quantities. By plotting  $J(\langle\phi\rangle)$  versus  $\langle\phi\rangle$  one can obtain the effective (renormalized) potential by integrating:

$$V_{\text{eff}}(\phi) = \int_0^\phi d\langle\phi\rangle J(\langle\phi\rangle) \quad (2.9)$$

The effective potential for scalar field theory is given by

$$V_{\text{eff}}(\phi) = \frac{m_R^2}{2} Z_\phi^{-1} \phi^2 + \frac{\lambda_R}{24} Z_\phi^{-2} \phi^4 \quad (2.10)$$

with renormalized mass  $m_R$ , renormalized coupling constant  $\lambda_R$  and field strength renormalization constant  $Z_\phi$ . The form of  $V_{\text{eff}}$  can be found e.g. in Ryder (1985)[R].

A typical example for the external source versus the expectation value and for the corresponding effective potential versus  $\phi$  is shown in figure 6 and 7 for unbroken (UBS) and in figure 8 and 9 for spontaneously broken symmetry (SBS) respectively.

The field strength renormalization constant and the renormalized coupling can be extracted by fitting a function of the form

$$f(\langle\phi\rangle) = f_1 \langle\phi\rangle + \frac{f_2}{6} \langle\phi\rangle^3 \quad (2.11)$$

to  $J(\langle\phi\rangle)$ , where  $f_1$  and  $f_2$  are fit parameters. Comparing with the derivative of equation 2.10,  $Z_\phi$  is given by  $Z_\phi = \frac{m_R^2}{f_1}$  where  $m_R$  is given by calculations of the 2-point correlator, and  $\lambda_R$  is given by  $\lambda_R = f_2 Z_\phi^2$ .

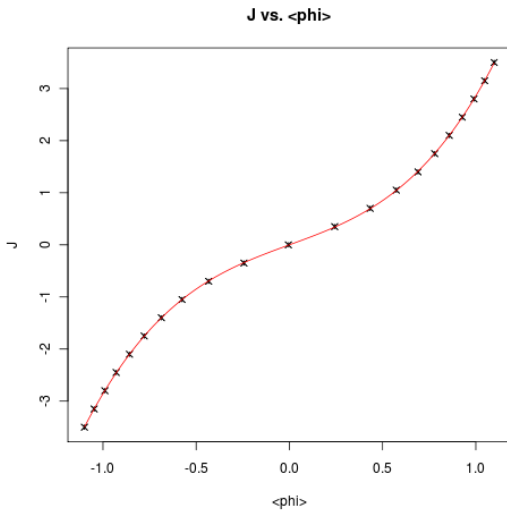


Fig. 6:  $J(\langle\phi\rangle)$  versus  $\langle\phi\rangle$  (UBS)

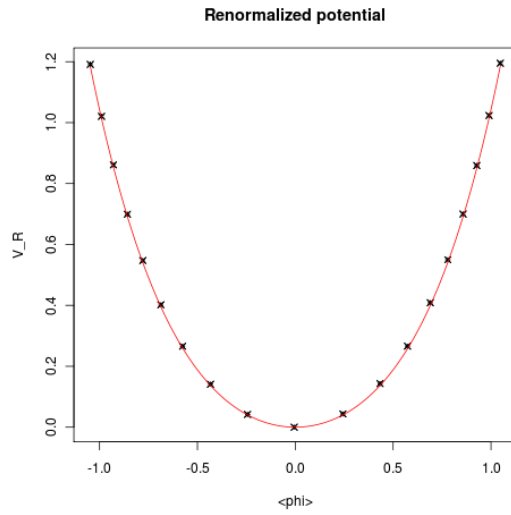


Fig. 7:  $V_{\text{eff}}(\phi)$  versus  $\phi$  (UBS)

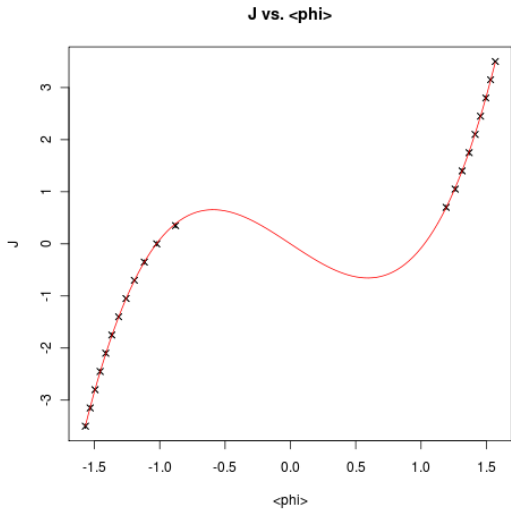


Fig. 8:  $J(\langle\phi\rangle)$  versus  $\langle\phi\rangle$  (SBS)

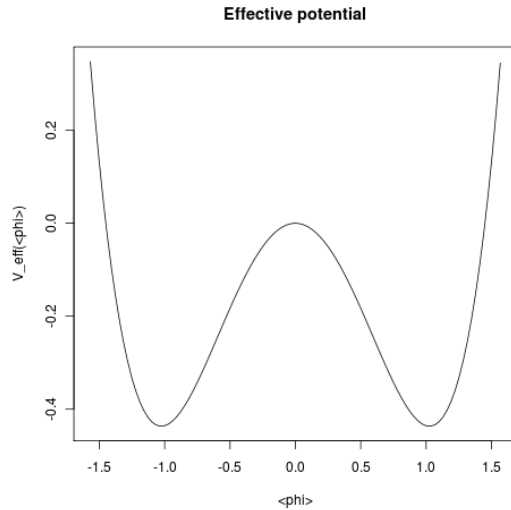


Fig. 9:  $V_{\text{eff}}(\phi)$  versus  $\phi$  (SBS)

A further discussion and additional plots are given in section 4.

### 3 Algorithm

We define a four-dimensional field with  $N^4$  lattice points. The lattice spacing is  $a$ . The derivatives are chosen  $\partial_\mu\phi(x) = \frac{1}{a}(\phi(x+a\hat{\mu}) - \phi(x))$  with  $\hat{\mu}$  the unit vector in  $\mu$ -direction. To be able to differentiate the field at the boundaries, we impose periodic boundary conditions. The field sites  $\phi(x)$  are initialized to a constant, say zero.

The basic idea of our algorithm (following METROPOLIS et al.) is summarized as follows

1. At the lattice position  $i$ , do a random variation of  $\phi_i$  to  $[\phi_i - d, \phi_i + d]$  for some parameter  $d$
2. Calculate the change in the action  $\Delta S$
3. Accept the change with a probability of  $\rho = \min(1, e^{-\Delta S})$

This procedure applied to all  $N^4$  lattice sites is called a sweep. A suitable value for the variation  $d$  can be found under the condition that the overall acceptance probability  $p$  in one sweep should be approximately 80%. If  $p < 0.78$ , the variation is too large and  $d$  is lowered by a factor of 0.95. If  $p > 0.82$ ,  $d$  is raised by a factor of 1.05. This is repeated for a certain number  $g_0$  of sweeps. The whole procedure of  $g_0$  sweeps can be understood as a “warming up” of the lattice. We observe that  $d \approx 0.3$  results from this procedure in almost every case.

The correlation function (3.1) between timelike intervals is the quantity of interest.

$$C(t) = \sum_x \langle 0 | \phi(t' + t, x) \phi(t', x) | 0 \rangle \quad (3.1)$$

This notation refers to the canonical quantization formalism where  $\phi$  is an operator. In our case, we just sum over the products of field values at different time gaps  $t$ . Any  $t'$  can be used for this calculation and in fact we use all of them to calculate an average for  $C(t)$ . Since the boundaries are periodic, the longest time gap in the lattice is  $t_N/a = N/2$  if  $N$  is even,  $(N-1)/2$  if it's odd.  $C(t_N + 1a)$  would be the same as  $C(t_N - 1a)$  for even  $N$  (for odd  $N$   $C(t_N + 1a) = C(t_N)$ ). To obtain a normalized correlation function we divide it by  $C(0)$ . We expect the function to drop like

$e^{-mt}$ , as is calculated e.g. in [PS], p.27. An example of  $C(t)$  is shown in fig. 10. The exponential decay is confirmed and a fit gives a decay constant of 2.02. Since we used an  $N = 10$  lattice, the time gaps only range from 0 to 5.

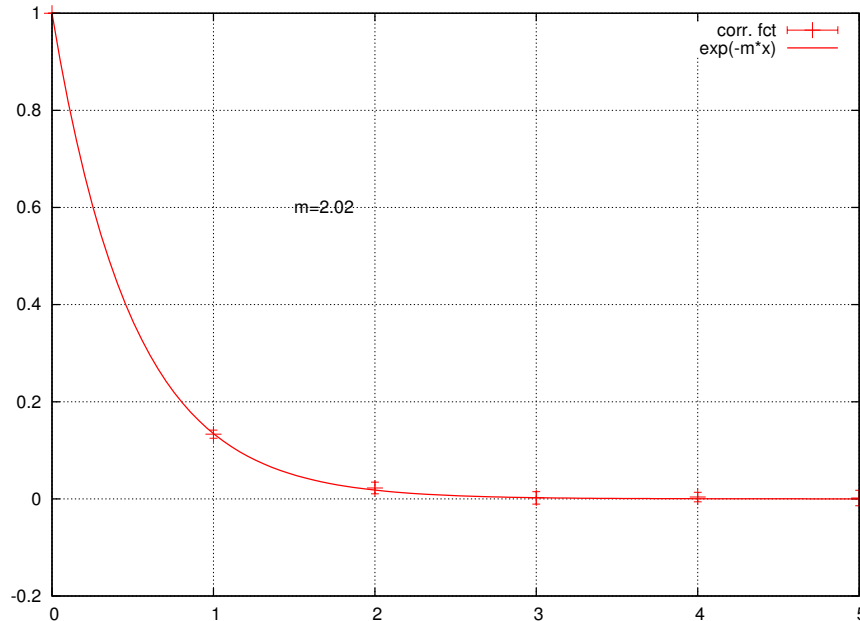


Fig. 10: Correlation function for  $\lambda = 1 = \mu^2 = a$ ,  $N = 10$

## 4 Data analysis

Several Monte-Carlo-Metropolis simulations have been started with different sets of parameters and different aims.

### 4.1 Mass calculation

Due to loop corrections for the propagator, shown to first order in section 2.2, the physical or renormalized mass gets shifted. According to [HMP] the correlation function is expected to drop like  $e^{-m_r t}$  with the renormalized mass  $m_r$  of a particle described by the field. This implies

$$\log \frac{C(t)}{C(t+a)} = m_r a = m_{\text{eff}} \quad (4.1)$$

$m_r, t$  are dimensionful quantities, while the effective mass is dimensionless. Actually (4.1) is the way we determine  $m_{\text{eff}}$ . This method suffers from the problem that  $C(t)$  drops very fast. Dividing two small numbers by each other and taking the logarithm produces high errors. Also these small numbers sometimes fluctuate below zero (c.f. errorbars in fig. 10) and the calculation fails. Because of this,  $C(0)/C(1a)$  is in most cases the only usable pair, especially when the masses are high.

After warming up the lattice, our program performs another certain number of sweeps and calculates  $C(t)$  and  $m_{\text{eff}}$  after each. This gives a Markov chain of masses because each mass depends on the previous field configuration. This can be nicely observed in a mass vs. number of sweeps plot, where a continuous line can be drawn through the points. The autocorrelation has to be considered in the standard deviation, which is explained in section 5.2.

We are interested in  $m_{\text{eff}}$  depending on the input parameter  $\mu^2$ . Our program allows an automated repetition of the procedure described above for different  $\mu^2$ . An example is shown in fig. 11. We are especially interested in the phenomenon of spontaneous symmetry breaking (about which more later) which occurs for negative  $\mu^2$ . In fig. 11 we see a breakdown of the mass for a negative  $\mu^2 = -0.1$ . The reason for this is, that the field develops a non-zero vacuum expectation value. Every lattice site is highly correlated and eq. (3.1) gives large contributions to  $C(t)$  and results in a function like  $C(t) = c + Ae^{-bt}$  with an offset of  $c \approx 0.9$  and a corresponding small  $A$ . The exponential decay can still be observed, but the method of dividing the function as in (4.1) fails and gives almost zero numbers, which are unphysical and do not represent masses.

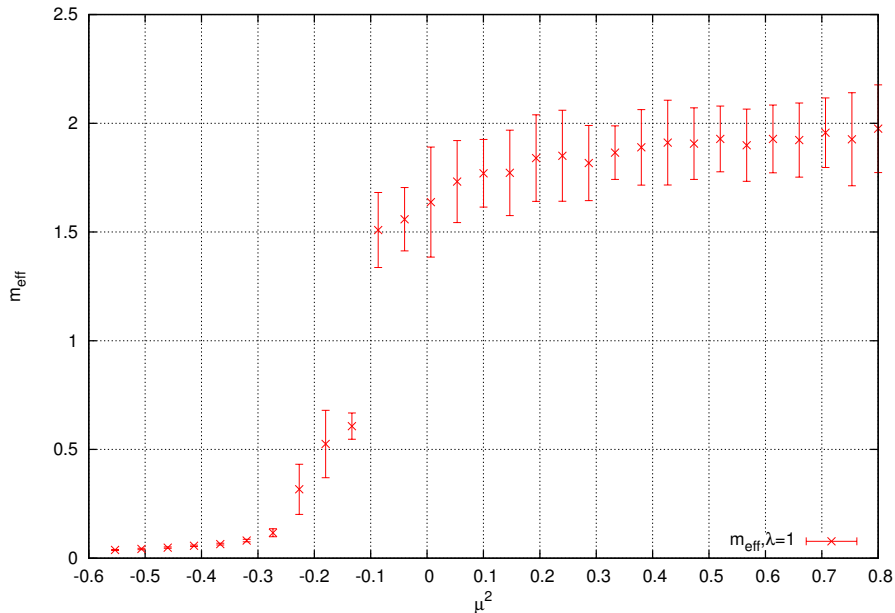


Fig. 11: Effective mass for different  $\mu^2$ .  $\lambda = 1, N = 10, a = 1$

Plots like fig. (11) are suited to determine the critical point where the phase transition occurs (in analogy to statistical mechanics one likes to speak of a broken and unbroken phase). Similar plots are shown in fig. 12 for higher couplings  $\lambda$ .

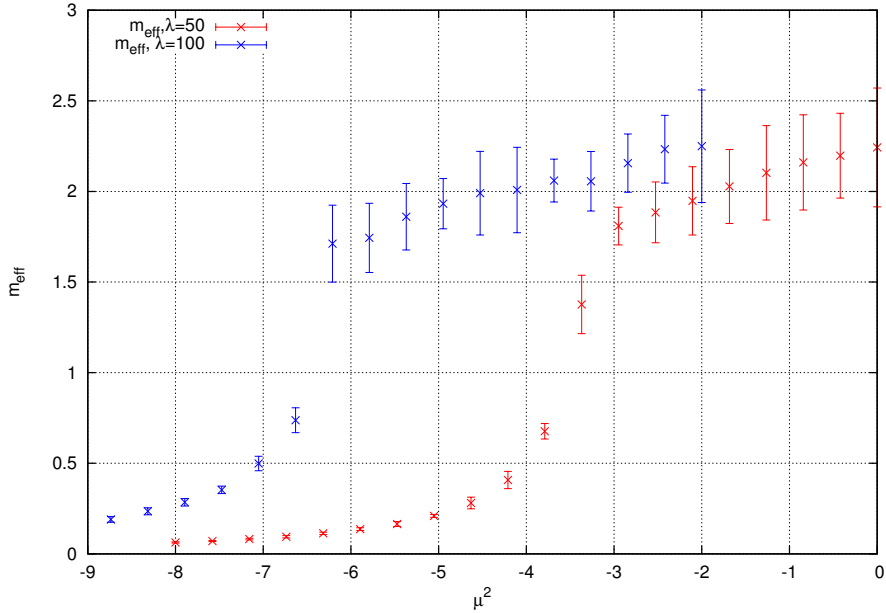


Fig. 12: Effective mass for different  $\mu^2$ .  $\lambda = 50(100)$ ,  $N = 10$ ,  $a = 1$

The critical points are at  $\mu_0^2 \approx -3$  for  $\lambda = 50$  and  $\mu_0^2 \approx -6.2$  for  $\lambda = 100$ . This suggests a roughly linear dependence of  $\mu_0^2$  on  $\lambda$ . The masses on the other side of the critical point are supposed to become higher with growing  $|\mu^2|$  (c.f. [HMP]). It would be an interesting addition to investigate them. One could either subtract the vacuum expectation value  $\phi_0$  in the calculation of  $C(t)$ , which corresponds to expanding around the vev like  $\phi(x) = \phi_0 + \eta(x)$  in perturbation theory, or one could perform an exponential fit to the unchanged  $C(t)$  of the form  $c + Ae^{-mt}$ . These features require an extensive restructuring of our program as it is and are thus not implemented.

To conclude this section we want to focus on the development of the vacuum expectation value of the field. The configuration of the field itself is not very descriptive. One can visualize a cross section of the  $xy$ -plane for example, but since the lattice size in one dimension is quite small (about 10) it doesn't look very smooth. Going to higher  $N$  significantly increases the computation time ( $\mathcal{O}(N^4)$ !). The average field (=vev if  $J = 0$ ) gives a much better insight to the internals of the field and is shown in fig. 13.

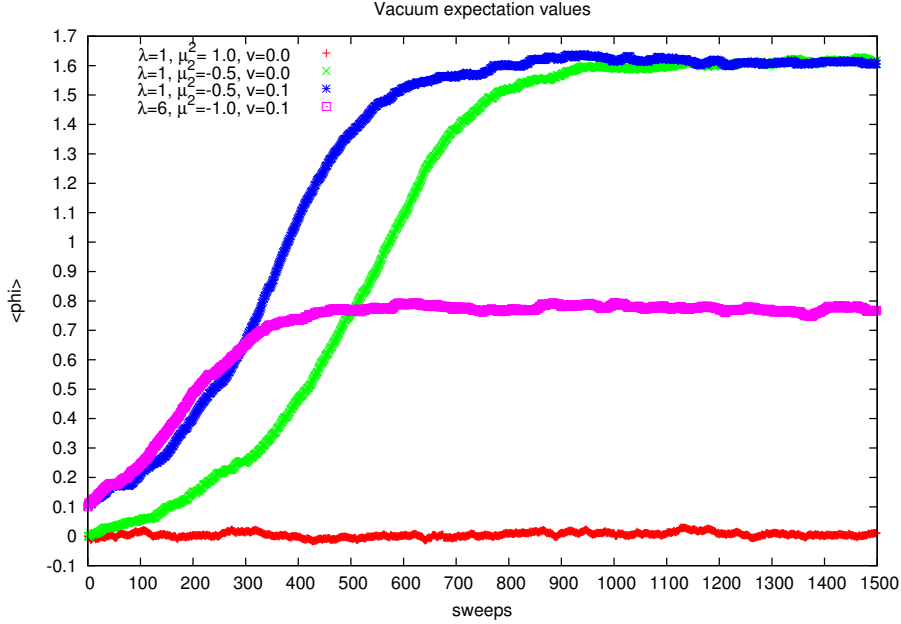


Fig. 13: Vacuum expectation value. The field is initialised to  $v$ .

The red line shows the field average for  $\lambda = \mu^2 = 1$  when  $\phi(x)$  is initialized to 0 (parameter  $v$  in the legend). It fluctuates a little around 0. The green line has  $\mu^2 = -0.5$  and lies within the broken phase. As the sweeps go up, the vev does too until it reaches a stable point after  $\approx 1000$  sweeps. This is the warmup phase. In comparison, the blue line was initialised at  $v = 0.1$  and reaches the stable point earlier. The figure shows that  $g_0 > 1000$  is a good choice. When we start the simulation with  $v = 0$  several times, the stable point is reached equally often at the negative vev. This is what “spontaneous” breaking means. Setting  $v$  positive is like tipping the ball in the positive potential well. The choice has no influence on the mass. The fourth purple line shows that the vev at a special choice of  $\lambda = 6, \mu^2 = -1$  is about 0.8. The naive assumption would be a vev of  $\sqrt{-6\mu^2/\lambda} = 1$  which is only correct in zeroth-order perturbation theory without any mass shifts. Here these shifts also lead to a shifted vev.

## 4.2 Effective potential

The effective potential and the dependence of the expectation value  $\langle\phi\rangle$  on the external source  $J$  have been calculated for  $\lambda = 1$  and  $\lambda = 100$  for spontaneously broken and for unbroken symmetry each. Figures 14 and 15 show plots for the dependence of  $J$  on  $\langle\phi\rangle$  (inverted) for  $\lambda = 1$  and  $\mu^2 = -0.03$  and  $\mu^2 = -0.15$  respectively. The symmetry is spontaneously broken for  $\mu^2 = -0.15$  and remains unbroken for  $\mu^2 = -0.03$ , meaning that SSB occurs almost immediately as  $\mu^2 < 0$ . This is the consequence of a small mass shift due to a small coupling constant.

The corresponding effective potentials are given below in figures 16 and 17. Data points are omitted due to a reason given at the end of this chapter.

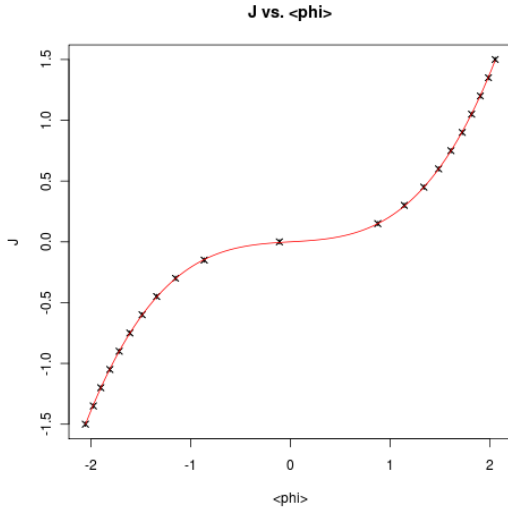


Fig. 14:  $J(\langle\phi\rangle)$  for  $\lambda = 1$  with UBS ( $\mu^2 = -0.03$ )

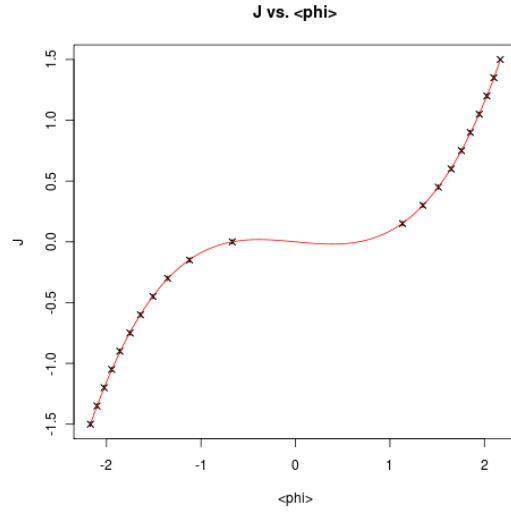


Fig. 15:  $J(\langle\phi\rangle)$  for  $\lambda = 1$  with SBS ( $\mu^2 = -0.15$ )

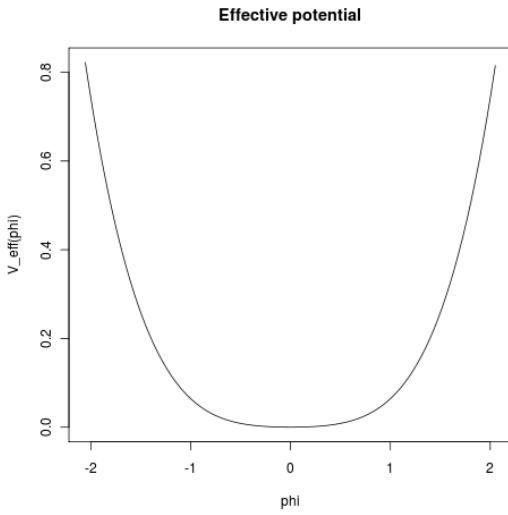


Fig. 16:  $V_{\text{eff}}$  for  $\lambda = 1$  with UBS ( $\mu^2 = -0.03$ )

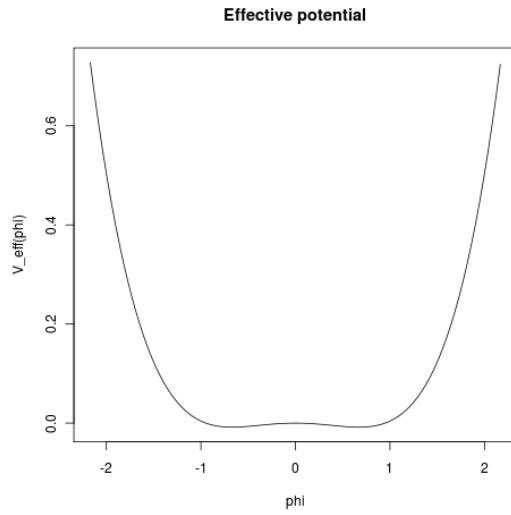


Fig. 17:  $V_{\text{eff}}$  for  $\lambda = 1$  with SBS ( $\mu^2 = -0.15$ )

The situation changes for  $\lambda = 100$ . Figure 18 shows  $J(\langle\phi\rangle)$  for  $\mu^2 = -5.0$ . Even for such small  $\mu^2$  no symmetry breaking occurs because of a large mass shift! The symmetry remains unbroken until  $\mu^2 \lesssim -6.2$  as predicted by calculations of the renormalized mass (see section 4.1). For  $\mu^2 = -6.5$  the plot of  $J(\langle\phi\rangle)$  is given in figure 19. Again the corresponding effective potentials are given below in figures 20 (UBS) and 21 (SBS).

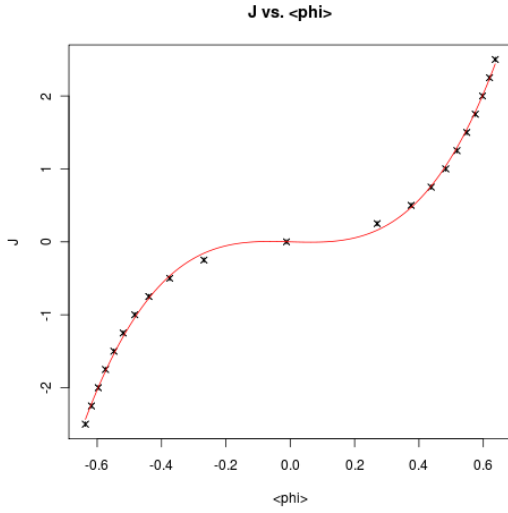


Fig. 18:  $J(\langle\phi\rangle)$  for  $\lambda = 100$  with UBS ( $\mu^2 = -5.0$ )

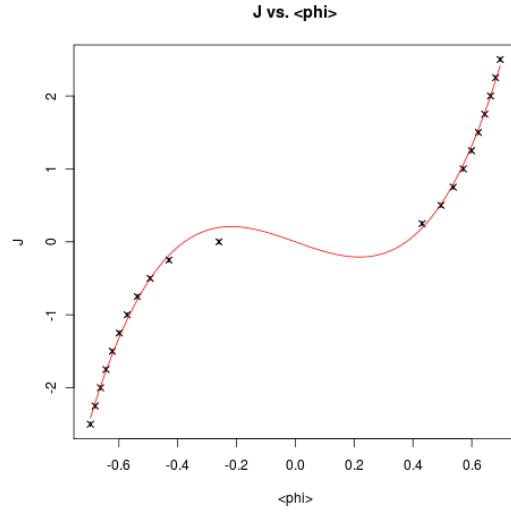


Fig. 19:  $J(\langle\phi\rangle)$  for  $\lambda = 100$  with SBS ( $\mu^2 = -6.5$ )

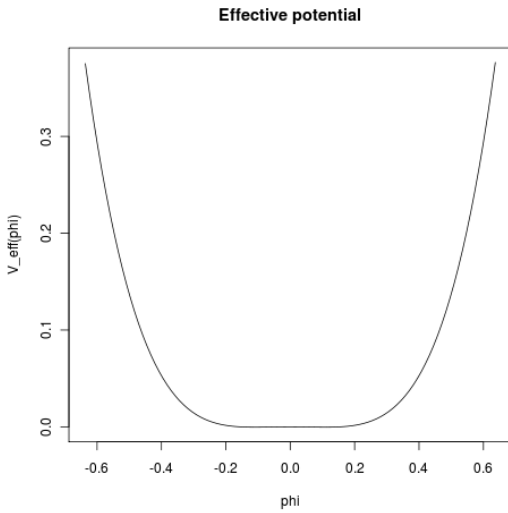


Fig. 20:  $V_{\text{eff}}$  for  $\lambda = 100$  with UBS ( $\mu^2 = -5.0$ )

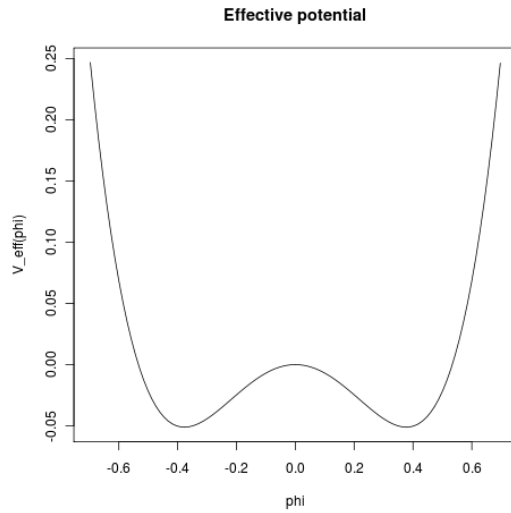


Fig. 21:  $V_{\text{eff}}$  for  $\lambda = 100$  with SBS ( $\mu^2 = -6.5$ )

#### 4.2.1 Errors of numerically calculated $V_{\text{eff}}$

As mentioned before, data points have been omitted for the effective potentials. The reason is, that we used the trapezoid rule for calculating the effective potential numerically, which is only valid for small spacings between the data points. For  $\mu^2 < 0$  we observed, that these spacings vary more strongly than for  $\mu^2 > 0$ . Thus the error for the trapezoid rule becomes much larger. An example for an effective potential with  $\mu^2 > 0$  is given in section 2.4 in figure 7. The integration of the fitted function for  $J(\langle\phi\rangle)$  and the numerically integrated  $J(\langle\phi\rangle)$  coincide well. Figures 22 and 23 show the effective potentials for  $\mu^2 < 0$  calculated with both methods. While for unbroken symmetry

small deviations can be observed, the trapezoid rule fails totally if the symmetry is spontaneously broken.

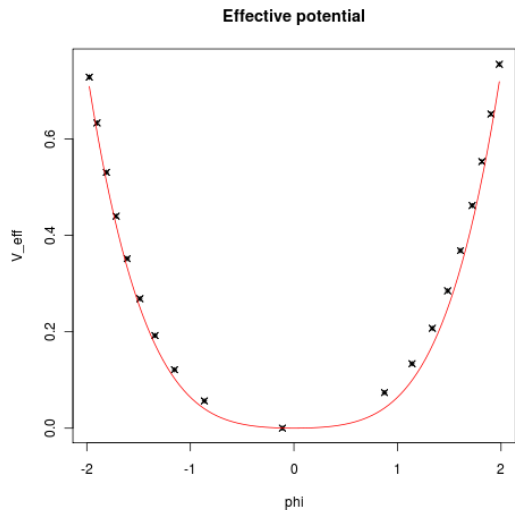


Fig. 22:  $V_{\text{eff}}$  for  $\lambda = 1$  with UBS  
( $\mu^2 = -0.03$ )

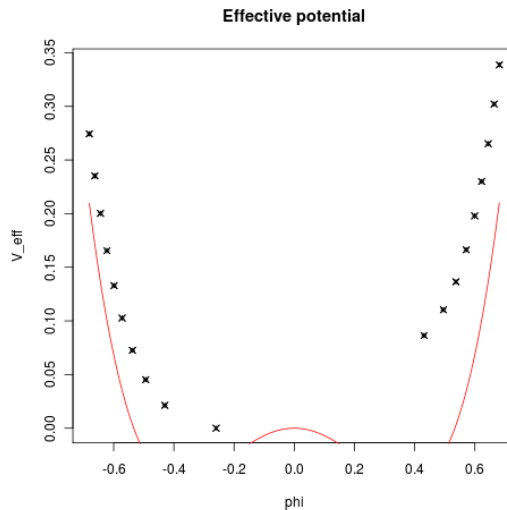


Fig. 23:  $V_{\text{eff}}$  for  $\lambda = 100$  with SBS  
( $\mu^2 = -6.5$ )

### 4.3 Renormalized coupling constant

As described in section 2.2, the physical coupling constant is shifted away from the coupling parameter  $\lambda$  in the Lagrangian as a consequence of renormalization. With use of the effective potential or, more specific, the dependence of  $J$  on  $\langle\phi\rangle$ , one is able to calculate the renormalized coupling and the field strength renormalization constant as depicted in section 2.4. For  $\mu^2 = 1.0\dots 1.64$  and  $\lambda = 10$ , tables 1, 2 and 3 list how  $m_R$ , the fit parameters for the  $J(\langle\phi\rangle)$  fit and  $Z_\phi$  depend on  $\mu^2$ .

$m_R$	2.122	2.140	2.167	2.185	2.201
$\Delta m_R$	0.006	0.006	0.009	0.009	0.006
$\mu^2$	1.000	1.160	1.320	1.480	1.640

Table 1:  $m_R$  vs.  $\mu^2$

$f_1$	$\Delta f_1$	$f_2$	$\Delta f_2$	$\mu^2$
1.550	0.003	8.927	0.017	1.000
1.707	0.003	8.922	0.026	1.160
1.853	0.003	8.963	0.023	1.320
2.013	0.003	8.919	0.023	1.480
2.160	0.003	8.973	0.025	1.640

Table 2: Fitparameters vs.  $\mu^2$

$Z_\phi$	2.905	2.682	2.535	2.372	2.244
$\Delta Z_\phi$	0.017	0.017	0.020	0.019	0.012
$\mu^2$	1.000	1.160	1.320	1.480	1.640

Table 3:  $Z_\phi$  vs.  $\mu^2$

The dependence of  $m_R$  on  $\mu^2$  is graphically shown in fig. 24 and the dependencies of  $Z_\phi$  and  $\lambda_R$  on  $m_R$  in figs. 25, 26.

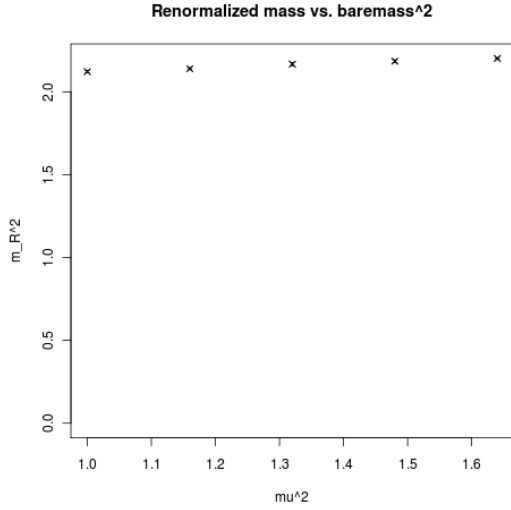


Fig. 24:  $m_R$  vs.  $\mu^2$  for  $\lambda = 10$

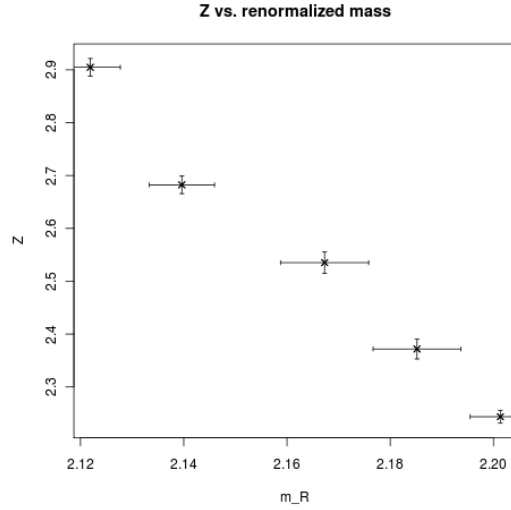


Fig. 25:  $Z_\phi$  vs.  $m_R$  for  $\lambda = 10$

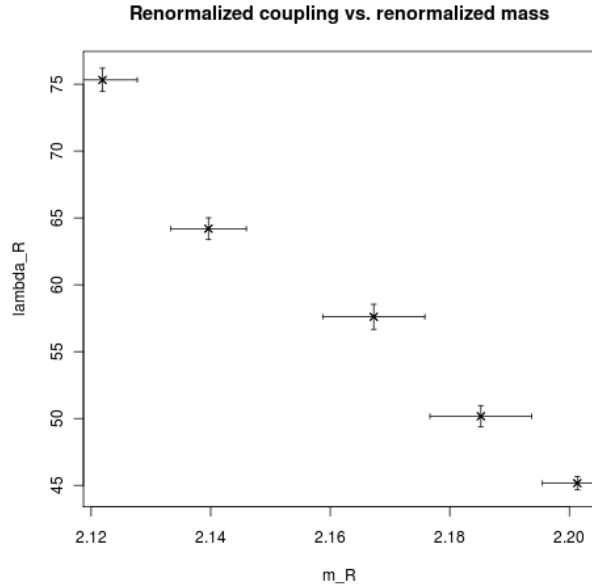


Fig. 26:  $\lambda_R$  vs.  $m_R$  for  $\lambda = 10$

Substantial is the strong dependence of  $\lambda_R (Z_\phi)$  on  $m_R$ . Unfortunately we have no other data to compare our results with. A possible explanation for this behaviour is given by the following argumentation: The shift of the coupling constant is due to loop corrections. These corrections take place at energies below a defined cut-off energy (momentum) (c.f. section 2.2). The larger the mass of the exchanged particle (scalar particle) the smaller is the phase space, i.e. the possible momentum states for the process to take place. This has the consequence, that the shift of the coupling constant becomes smaller.

## 4.4 Finite size effects

In this chapter we want to study the dependence of the results of our algorithm on the size of the lattice. The spacing  $a$  is held constant while the total size  $N$  is varied. As an observable we choose the effective mass and calculate it in a range of  $N = 5$  up to  $N = 25$  (fig. 27). As one can see, low  $N$  produce high fluctuations. Below  $N = 5$  calculations were impossible because  $C(1a)$  tends to go negative just by fluctuating. With increasing  $N$ , the errorbars indicate an improved accuracy.  $N$  is the crucial value for computing runtime – The last point in this plot took approx. 30 minutes. This is why in most of our calculations we used  $N = 10$  which has quite large errorbars, but gives reasonable runtimes.

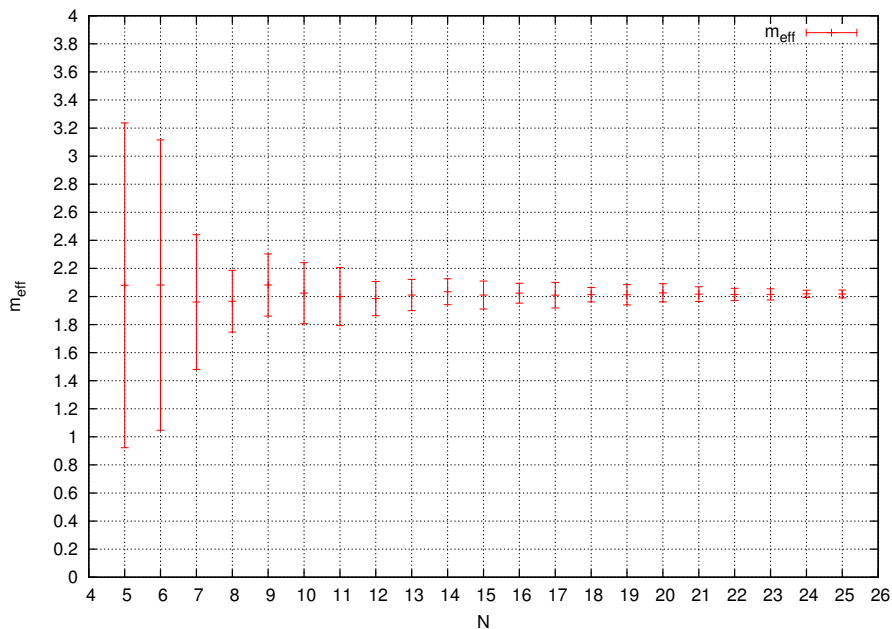


Fig. 27: Finite size effects: Mass depending on  $N$

## 5 Error analysis

### 5.1 Standard deviation

An unbiased estimator of the standard deviation of a sample  $x_i, 1 = 1 \dots N$  is

$$\sigma = \sqrt{\frac{1}{N-1} \sum_i (x_i - \bar{x})^2} \quad (5.1)$$

where  $\bar{x}$  is an estimator of the mean.

The standard deviation of the mean is smaller by a factor of  $1/\sqrt{N}$ .

$$\sigma_{\text{mean}} = \frac{\sigma}{\sqrt{N}} \quad (5.2)$$

## 5.2 Autocorrelation

To calculate the standard deviation of a series  $X_i$  of autocorrelated masses, we use the `acf`-function of  $R$  to get the normalized autocorrelation function  $\Gamma(t)$  of the series. Then the normal standard deviation (`sd` function) has to be multiplied by a factor of  $\sqrt{2\tau_{\text{int}}}$  with the integrated correlation time

$$\tau_{\text{int}} = \frac{1}{2} \sum_{t=-\infty}^{\infty} \Gamma(t) = \frac{1}{2} + \sum_{t=1}^{\infty} \Gamma(t). \quad (5.3)$$

$\Gamma(-t) = \Gamma(t)$  is assumed.

## 6 Summary

Quantum field theory on a lattice is a useful application of MC methods and an important assistance for continuum theory.  $\phi^4$  theory shows to be a very deep topic, although it is the simplest of field theories, especially because of the occurrence of spontaneous symmetry breaking. Being the Lagrangian of the Higgs field in the Standard Model, (1.1) is related to the very frontier of particle physics research. Simulations like ours can be used to simulate whether the Higgs mechanism could actually work (which was done in the paper [HMP]). Our simulation of course reaches lower goals and is able to locate the critical value of spontaneous symmetry breaking. Effective masses can be calculated in the unbroken phase, and, with extension suggestions made in 4.1, for the broken phase. The effective potential is a efficient way to extract other quantities like renormalized coupling constants and the field strength renormalization constant  $Z_\phi$ . Also it gives a nice visualization of broken symmetry (“Mexican hat”).

The key issues we encountered during the programming are

- Computation time governed by  $N^4$
- Warming up the lattice needs  $> 1000$  sweeps
- Mass/coupling shifts due to renormalization manifest themselves
- Low  $N$  give bad accuracy (finite size effects)
- Calculated masses fluctuate a lot (errorbars) and are autocorrelated
- Continuum limit  $a \rightarrow 0$  can be extrapolated

A personal impression of the project for us is to see that the path integral formalism actually works and is able to confirm the spontaneous symmetry breaking.

## References

- [CF] Creutz, Freedman: Statistical approach to quantum mechanics
- [M] Montvay: Quantum fields on a lattice
- [R] Lewis H. Ryder: Quantum field theory(1985)
- [PS] Peskin, Schröder: Introduction to Quantum Field Theory (1995)
- [HMP] Huang, Manousakis, Polonyi: Effective Potential in scalar field theory, Physical Review D (1987)

## List of Figures

1	Loop diagrams of the 2-pt. function . . . . .	2
2	4-point corrections, one loop . . . . .	2
3	Finite lattice spacing . . . . .	2
4	Unbroken symmetry . . . . .	3
5	Spontaneously broken symmetry . . . . .	3
6	$J(\langle\phi\rangle)$ versus $\langle\phi\rangle$ (UBS) . . . . .	4
7	$V_{\text{eff}}(\phi)$ versus $\phi$ (UBS) . . . . .	4
8	$J(\langle\phi\rangle)$ versus $\langle\phi\rangle$ (SBS) . . . . .	5
9	$V_{\text{eff}}(\phi)$ versus $\phi$ (SBS) . . . . .	5
10	Correlation function for $\lambda = 1 = \mu^2 = a, N = 10$ . . . . .	6
11	Effective mass for different $\mu^2$ . $\lambda = 1, N = 10, a = 1$ . . . . .	7
12	Effective mass for different $\mu^2$ . $\lambda = 50(100), N = 10, a = 1$ . . . . .	8
13	Vacuum expectation value . . . . .	9
14	$J(\langle\phi\rangle)$ for $\lambda = 1$ with UBS ( $\mu^2 = -0.03$ ) . . . . .	10
15	$J(\langle\phi\rangle)$ for $\lambda = 1$ with SBS ( $\mu^2 = -0.15$ ) . . . . .	10
16	$V_{\text{eff}}$ for $\lambda = 1$ with UBS ( $\mu^2 = -0.03$ ) . . . . .	10
17	$V_{\text{eff}}$ for $\lambda = 1$ with SBS ( $\mu^2 = -0.15$ ) . . . . .	10
18	$J(\langle\phi\rangle)$ for $\lambda = 100$ with UBS ( $\mu^2 = -5.0$ ) . . . . .	11
19	$J(\langle\phi\rangle)$ for $\lambda = 100$ with SBS ( $\mu^2 = -6.5$ ) . . . . .	11
20	$V_{\text{eff}}$ for $\lambda = 100$ with UBS ( $\mu^2 = -5.0$ ) . . . . .	11
21	$V_{\text{eff}}$ for $\lambda = 100$ with SBS ( $\mu^2 = -6.5$ ) . . . . .	11
22	$V_{\text{eff}}$ for $\lambda = 1$ with UBS ( $\mu^2 = -0.03$ ) . . . . .	12
23	$V_{\text{eff}}$ for $\lambda = 100$ with SBS ( $\mu^2 = -6.5$ ) . . . . .	12
24	$m_R$ vs. $\mu^2$ for $\lambda = 10$ . . . . .	13
25	$Z_\phi$ vs. $m_R$ for $\lambda = 10$ . . . . .	13
26	$\lambda_R$ vs. $m_R$ for $\lambda = 10$ . . . . .	13
27	Finite size effects: Mass depending on $N$ . . . . .	14

## List of Tables

1	$m_R$ vs. $\mu^2$ . . . . .	12
2	Fitparameters vs. $\mu^2$ . . . . .	12
3	$Z_\phi$ vs. $\mu^2$ . . . . .	13